

# Climate change induces extreme soil droughts in Europe

L. Samaniego<sup>1,\*,+</sup>, S. Thober<sup>1,+</sup>, R. Kumar<sup>1</sup>, N. Wanders<sup>2</sup>, O. Rakovec<sup>1,\*\*\*</sup>, M. Pan<sup>3</sup>, M. Zink<sup>1,\*\*</sup>, J. Sheffield<sup>4</sup>, E. F. Wood<sup>3</sup>, and A. Marx<sup>1</sup>

<sup>1</sup>UFZ-Helmholtz Centre for Environmental Research, Leipzig, Germany

<sup>2</sup>Utrecht University, Physical Geography, Utrecht, Netherlands

<sup>3</sup>Princeton University, Civil and Environmental Engineering, Princeton, NJ, United States

<sup>4</sup>University of Southampton, Geography and Environment, UK

\*\*Now at European Centre for Medium-Range Weather Forecasts, Reading, UK

\*\*\*Czech University of Life Sciences, Faculty of Environmental Sciences, Prague, Czech Republic

+These authors contributed equally to this work.

\*luis.samaniego@ufz.de

**Global warming may exacerbate soil moisture droughts. However, evaluations of future droughts are not conclusive because of the uncertainty in estimates of future warming. Here, we estimate the impacts of differential climate change at 1-3 K on the largest soil moisture droughts across Europe to understand the implications of the goal of the 2015 Paris climate change agreement to constrain global warming to below 1.5 degrees. The results show that under an increase of 3 K compared to 1.5 K, drought area will increase by 40% ( $\pm 24\%$ ) and will potentially affect 42% more people. Similarly, an event like the 2003 drought will become two times more frequent. Adapting to a temperature increase of 3 K implies adjusting to an increase**

**in aridity of up to 8%, which is comparable to the soil water deficit during the 2003 event. Consequently, any event of this magnitude will be too small to be classified as a drought in the future.**

**Keywords: Climate change, Agricultural drought, Soil Moisture Index (SMI), Aridity**

Global warming is projected to increase evaporation and to reduce soil moisture where it is present, at several hotspot locations around the globe<sup>1,2</sup>. Current research indicates that, although climate change may not create droughts, it may exacerbate them<sup>3-8</sup>. Consequently, droughts may set in more quickly, be more intense and last longer<sup>9</sup>. The recent Paris climate change agreement focuses on holding the global temperature increase to well below 2 K or even 1.5 K above pre-industrial levels<sup>10</sup>. It is worth noting that future global temperatures will likely exceed 2 K above pre-industrial levels by 2100<sup>11</sup>. Limiting global warming to these levels has unknown effects on the characteristics of soil moisture droughts (e.g., drought area and duration) because these characteristics have been quantified for different future periods using emission scenarios that cover a wide range of temperature projections<sup>9,12-15</sup>. Moreover, the definition of a drought under a non-stationary climate must be carefully chosen such that drought events represent dry anomalies with respect to reference conditions<sup>16</sup>. The agricultural adaptation potential has been estimated for Europe, taking into account crop yield and profit per hectare<sup>17</sup>. Here, we quantify the extent and duration of future droughts and changes in aridity for different warming levels with and without adaptation (see methods). We aim to provide information on the benefits of limiting global warming to 1.5 K relative to 3 K in terms of

agricultural droughts, which have substantial impacts on vegetation stress, crop losses, the risk of forest fires, tourism<sup>18</sup>, ecosystem services and greenhouse gas emissions<sup>19</sup>.

The uncertainty in climate projections and hydrological model parameterisations introduces considerable variability into the resulting projections of the characteristics of soil moisture drought<sup>20,21</sup>, thus highlighting the need for multi-model ensembles to enable comprehensive assessments of these events. However, studies of soil moisture droughts at continental and global scales are limited to a few ensemble members and/or employ a single hydrological model<sup>22</sup>. Existing multi-model analyses of future droughts focus primarily on hydrological droughts<sup>13,21</sup>.

To address these shortcomings, we establish a modelling chain using multiple models to generate an unprecedentedly large (60-member) ensemble of high-resolution  $5 \times 5 \text{ km}^2$  hydrological simulations that cover the European domain (see methods). We use two hydrological models (HMs) and two land surface models (LSMs) that employ a consistent set of land-surface properties. The two hydrologic models use a temperature-based PET scheme, which has been criticised within the application of drought analysis using the Palmer Drought Severity Index (PDSI)<sup>6,23</sup>. The soil moisture index (SMI) derived from these HMs, however, do not show the same deficiency as the PDSI because of methodological differences on how these indices are estimated (see methods). All HMs/LSMs are driven by downscaled forcings obtained from five bias-corrected Coupled Model Inter-comparison Project Phase 5 (CMIP5) projections<sup>24</sup> that follow three representative con-

centration pathways (RCPs; RCP2.6, RCP6.0, and RCP8.5). To guarantee the comparability across the multi-model ensemble, all HMs and LSMs estimate soil moisture up to a depth of 2 m and the estimated soil moisture values are transformed into a monthly soil moisture index (SMI)<sup>20</sup>. These high resolution SMI fields are required to perform a spatio-temporal drought cluster analysis<sup>20</sup> which enables to quantify the area-duration characteristics of every soil moisture drought event. Based on this cluster analysis, two key drought characteristics, the area under drought and the drought duration, are estimated for all drought events simulated by each general circulation model (GCM) and HM/LSM model combination(see methods). These two characteristics are then analysed for the largest drought within each GCM-HM/LSM combination over specific 30-year periods that correspond to different warming levels under the three RCPs<sup>25</sup>. A time sampling approach is used to extract future 30-year periods that correspond to global warming levels of 1.0, 1.5, 2.0, 2.5, and 3 K with respect to pre-industrial levels for each of the GCM/RCP projections<sup>15</sup> (see methods). The period from 1971 to 2000 is selected to represent present-day conditions.

Based on our multi-model ensemble analysis, Figure 1a shows that the ensemble median of the largest drought areas increases from 18.7 % of the European territory under a warming of 1.5 K to 26.2 % under a warming of 3 K. The drought threshold from the reference period 1971-2000 is used to enable comparison with historic events; that is, adaptation to climate change is not considered. If adaptation is not considered, then only the top 10 % of simulated drought areas under a warming of 1.5 K exceed the ensemble

median under a global warming of 3 K. Note that the percentage of ensemble members that exceed the median of the 3 K ensemble increases non-linearly with the degree of global warming. For example, this quantity increases by 13.3 % (2.5 % to 15.8 %) as the amount of global warming increases from 1 K to 2 K; however, it increases by 34.2 % as the amount of global warming increases from 2 K to 3 K.

Drought duration (Figure 1c) also exhibits substantial changes across the different warming levels. The median duration of exceptional drought events shows approximately a two- to three-fold increase between the 1.5 and 3 K warming levels (i.e., it increases from 20 months under a warming of 1.5 K to approximately 55 months under a warming of 3 K). Given these changes in the distributions of the areas and the durations of extreme drought events, these future events may no longer represent droughts, which are defined as deviations from normal conditions. This analysis indicates that, for amounts of global warming equal to or greater than 1.5 K, the normal conditions that are used to define typical drought characteristics must be reassessed.

The impact of climate change on drought characteristics is strongly diminished after adaptation to drought events is considered (i.e., the soil moisture drought threshold is re-calculated based on the projected soil moisture, as indicated in the methods section). Overall, the ensemble median drought area is estimated to be between 16 % and 18 % of the European territory, and the duration is approximately 9 to 12 months for all of the considered warming levels . A significant difference is only found between the

warming levels of 3 K and at most 1.5 K (applying a Kolmogorov-Smirnov test with a significance level of 5%, Figure 1d). Ideally, it is expected that drought area and duration remain unchanged if the soil moisture drought threshold is estimated for each warming level separately (representing adaptation to climate change). Small deviations may still occur because of the intrinsic uncertainty of the processes describing the soil moisture dynamics. It is worth noting that these observed increases are independent of the chosen SMI drought threshold (see methods, cf. Figure 1 and Figure S1.)

The substantial increases in drought area and duration without adaptation (Figure 1a,c) are not evenly distributed across the European domain. Figure 2 depicts strong spatial differences in the drought area and duration over six major environmental regions in Europe (i.e., the Alpine North, Atlantic, Boreal, Continental, Mediterranean, and Alpine South regions; see the left panel of Figure 3)<sup>26,27</sup>. The exact values are provided in Table 1. The largest increases in the drought area and duration are projected to occur in the Mediterranean. Compared with the estimates for the historical period (1971–2000), the drought area will change from 28 % on average to 49 % under a warming of 3 K (Figure 2a,f). The increase in drought area is less than 10 % in the Atlantic, Continental, Alpine North and Alpine South regions. Increased precipitation will decrease the drought area in the Boreal region by about 3 % under a global warming of 3 K. Interestingly, the Alpine North regions show the highest percentage in drought area among all regions for the historic period 1971-2000 (Figure 2a), which highlights that droughts have a relatively higher spatial dependence in this region than in the other ones.

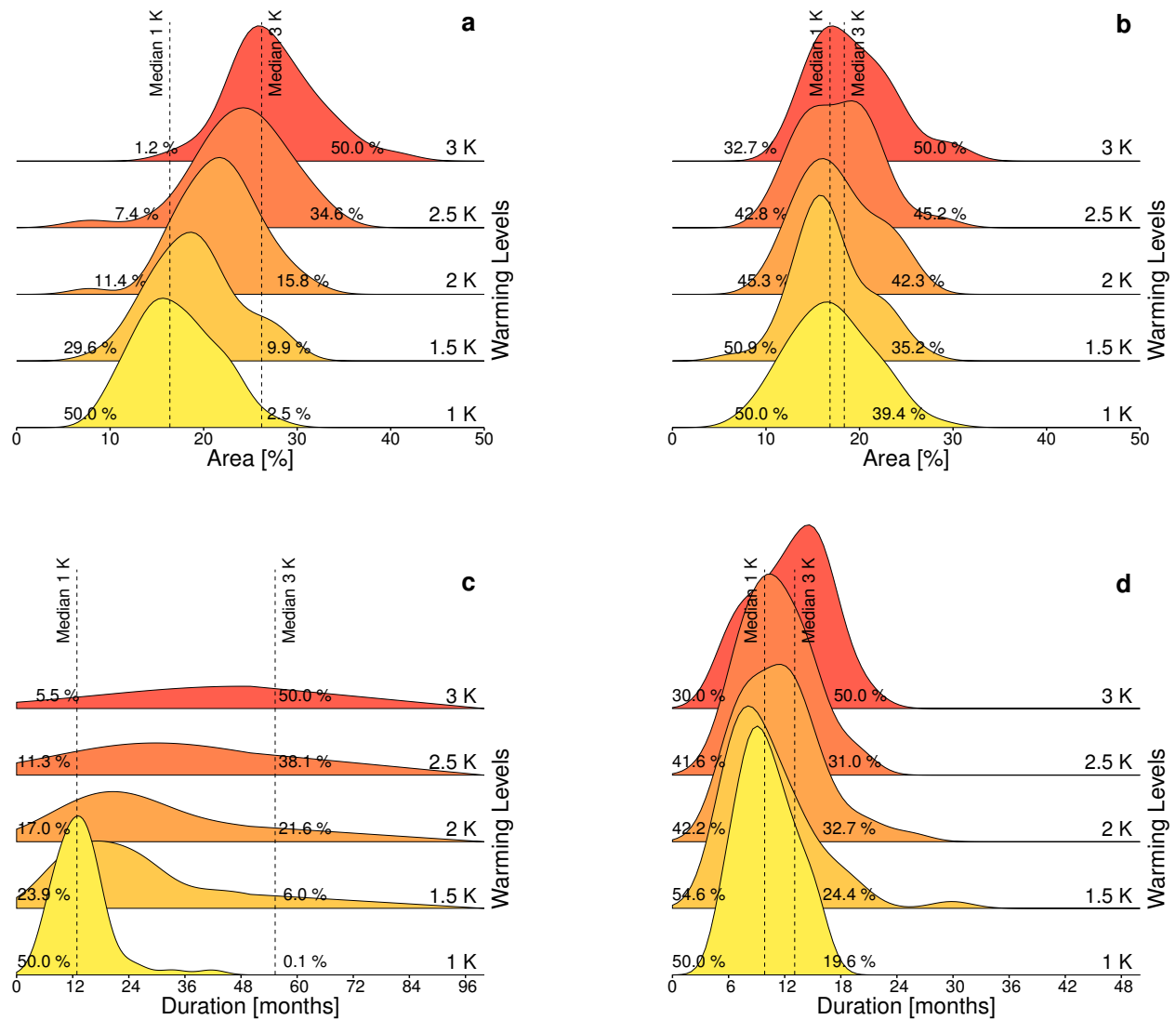


Figure 1: Distributions of the areal extents and durations of the most severe drought events that occur within Europe for different levels of global warming. Both drought characteristics are estimated for the largest drought event over the 30-year period corresponding to each global warming level and for each of the 60 members of the multi-model ensemble. Kernel density functions are then fitted to both the drought areas (a,b) and their durations (c,d). The results obtained using the drought threshold fixed to a reference period of 1971–2000, indicating no adaptation, are presented in the panels on the left-hand side (a,c). Recalculating the drought characteristics using an adaptive threshold for each warming period leads to the results presented in the right-hand panels (b,d). The vertical dashed lines indicate the median values for global warming amounts of 1 K and 3 K. The fractions of ensemble members located towards the tails are also denoted as percentages. The x-axis limits are different for the duration with and without adaptation (i.e., panels c and d) for clarity.

With the exception of the Alpine North and Boreal regions, the durations of the largest drought events are three to four times higher under a warming of 3 K compared to historical values (Table 1). The increases in drought duration are non-linearly related to climate change because they double (at most) under a global warming of 2 K. The longest droughts, which have durations exceeding 10 years (120 months), are projected to occur in the Mediterranean, Alpine South and Continental regions under a global warming of 3 K. Overall, our results show an alteration of the hydrologic regimes in the Mediterranean and Continental regions when a warming level of 3 K is approached.

The frequency of drought events (expressed in terms of the number of drought months occurring per year) also exhibits marked regional and sub-regional differences, due mainly to the influence of local physiographic and climatic characteristics (Figure 2 m-r). During the historical period, the mean drought frequency for all of the grid cells in all of the regions is approximately 2 months per year. This historically low value increases to an unprecedentedly high value under climate change, if no adaptation is considered. For example, the Mediterranean will experience a steady increase in this quantity as the warming level rises, reaching 5.6 months per year under 3 K. Note that some parts of the Iberian Peninsula are projected to experience more than seven drought months per year under the 3 K warming level (Figure 2r). These events may no longer be droughts, given that they occur half of the time. All HMs project increases in drought frequency in the Mediterranean, which is a result of the reduced precipitation in this region (see Figure S9 and ??). The Continental region shows a change from 1–2 months per year to



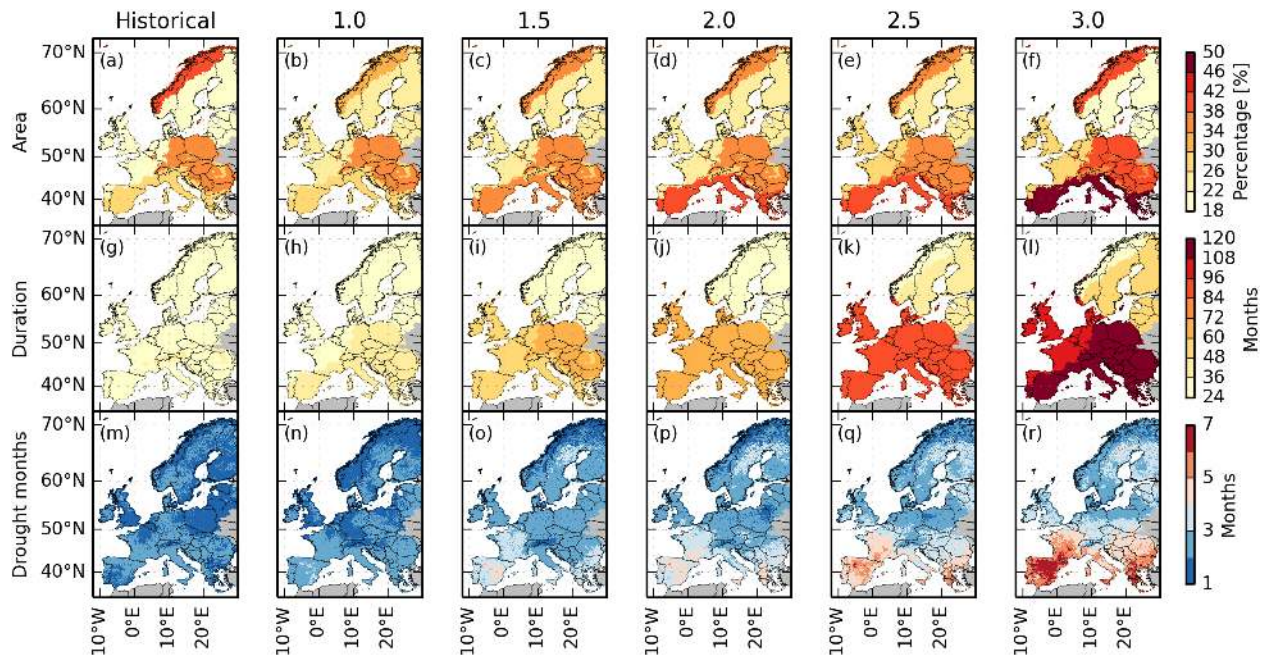


Figure 2: The area under drought evaluated for the European regions used in the Fifth Assessment Report of the Intergovernmental Panel on Climate Change (IPCC AR5) <sup>26</sup> and quantified as a percentage of the total area of each region (a–f). The drought duration is shown for the individual regions (g–l). The area under drought and the drought duration are calculated for the multi-model median of the largest drought events. The frequency of drought months is depicted at the individual grid cell level, which is calculated based on the multi-model median estimates (m–r). All of the results are calculated assuming no adaptation to climate change; i.e., a fixed drought threshold derived from the reference period 1971–2000 is used.

3–5 months. Most locations in the Alpine South region will experience a shift in drought frequency from 1–2 months under present-day conditions to 4 months per year under a warming of 3 K.

The previous two figures highlight the need for constant adaptation to the changing climate and indicate that historic drought thresholds may not apply in the future. <sup>14</sup> Adaptation of society to the new normal is known to be associated with substantial costs<sup>28</sup>.

However, the crucial question for society as a whole and water planners in particular is what the new drought conditions that will occur under different warming levels imply for adaptation policies. To answer this fundamental question, the change in the drought threshold in a 2-m deep soil column in litres per square metre (i.e., in millimetres of soil water storage) is estimated. This value is an indicator of the available soil water content under drought conditions and quantifies the change in aridity.

The resulting ensemble average change in the available soil water content is estimated over the six environmental regions for the different warming levels and seasons (i.e., winter, spring, summer, and autumn), including their variability and statistical significance. The magnitude of this change generally increases with increased global warming and is significant for changes larger than 3 % (Figure 3). Two major patterns are observed: 1) the Mediterranean and Atlantic regions experience decreases in soil water content in all seasons and under all warming levels; 2) the Alpine North, Alpine South, Boreal and Continental regions become wetter in winter and spring and drier in summer and autumn.

The Mediterranean region is the most affected in all seasons (Figure 3d), with the largest increase in aridity appearing in the winter and spring under all warming levels. At the 3 K warming level, the available soil water decreases by 35 mm ( $\pm 24$  mm), which corresponds to a shortage of  $35\,000\text{ m}^3\text{km}^{-2}$ . The Atlantic region exhibits the smallest changes in the available soil water among all of the regions and for all of the warming levels (Figure 3a). The Continental region exhibits positive changes during the winter for

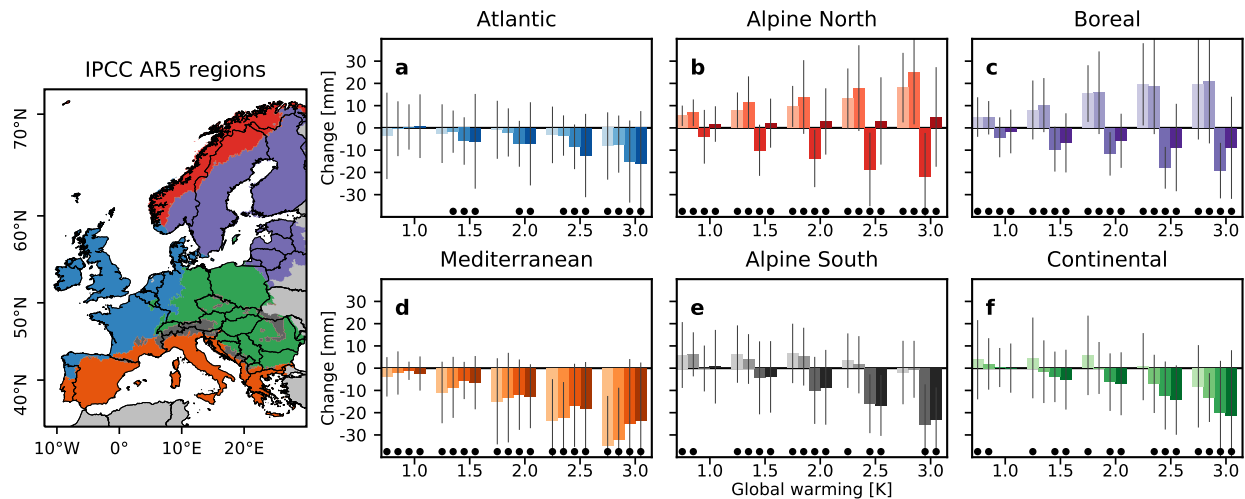


Figure 3: Changes in the soil water availability (increases in aridity) during drought events between a given warming level and the reference period, considering adaptation to climate change. The results are aggregated to the IPCC AR5 regions<sup>27</sup> (left panel; own graphics based on data provided by Marc J. Metzger, University of Edinburgh) for the different seasons (from left to right, DJF, MAM, JJA, and SON) and from for each warming level. The whiskers indicate the inter-quartile range of the multi-model ensemble results. The markers at the bottom of the plots indicate changes that differ significantly from zero, as determined using a Wilcoxon rank-sum test and a significance level of 5 %.

warming amounts of up to 2 K (Figure 3f). In contrast, negative changes are observed for all of the warming levels above 1.5 K during the spring, summer and autumn. Earlier onsets of snowmelt cause increases in the available soil water in the winter and spring for all of the warming levels in the Alpine North and Boreal regions (Figure 3b and c). These earlier onsets also lead to increases in aridity in these regions of up to 20 mm in summer, when snowmelt is no longer a source of water.

Global warming leads to significant intensification of European droughts, which con-

firms previous work<sup>6</sup>. We show that climate change has diverse regional and seasonal impacts on soil water availability across Europe. An increase in surface water availability has been reported for different warming levels for the Alpine and Boreal regions<sup>2</sup>. However, this increase is unevenly distributed over the year. Moreover, soil water availability appears to decrease significantly throughout Europe during the growing season (i.e., summer and fall). Economic assessments of climate change adaptation for the agricultural sector are often based on temperature-related characteristic curves<sup>17</sup>. These analyses could benefit from incorporating soil moisture because it constitutes the primary source of water for plant growth.

The exacerbation of drought conditions in the Mediterranean under global warming of 1.5 K and 2 K will be unprecedented since the last millennium<sup>22</sup>. If a global warming of 3 K is reached, southern Spain and probably Italy and Greece will turn “into a desert”<sup>29</sup>. This unprecedented change will also have severe impacts on Mediterranean vegetation and biodiversity, and, thus on ecosystems and their services. The strong reductions in soil water availability during dry periods are mostly related to decreases in precipitation and increases in evapotranspiration<sup>2</sup> (see Figures S2 and S3). The relatively high decreases in soil water availability noted in this region are related to the relatively high increases in the maximum daytime temperatures compared to other regions<sup>30</sup>. Whether economic adaptation assessments<sup>17</sup> can properly assess such severe changes remains an open question.. Note that, while we estimate soil moisture for a 2 m deep soil column, many plants, particularly crops, do not have roots that extend to that depth. Consequently, we

likely underestimate the effects of soil moisture droughts in the top-soil layers because these layers tend to dry faster than the lower soil layers<sup>8</sup>.

We relate our results to the 2003 drought event (estimated based on historical observations, see methods) to illustrate the severity of the projected changes. Agricultural droughts are intrinsically related to significant reductions of evapotranspiration and gross primary production (GPP), as well as the occurrence of heat waves. For example, Europe emitted an amount of carbon dioxide that corresponds to the amount that is normally sequestered in four years during the 2003 drought events<sup>19</sup>. In the future, drought events that are similar in magnitude and extent to that of 2003 will be twice as frequent. In detail, our results indicate that the increase in frequency, which is defined as the ratio of SMI under a warming of 3 K with respect to that of the reference period, is approximately 2.0 ( $\pm 0.33$ ). The estimated average soil water availability deficit during the 2003 drought event was 27.6 mm. The change in the drought threshold at a warming level of 3 K (Figure 3) is of the same order of magnitude as the average deficit during the 2003 event in most of the regions. This result implies that much of this event will not be classified as a drought in the future, and the projected droughts will be associated with substantially less available soil water than the 2003 event.

We estimate that 42 % ( $\pm 22$  %) more people will be located within areas enduring extreme droughts under a warming level of 3 K compared to a warming level of 1.5 K (170 million people vs. 120 million people, respectively; Figure 4). In contrast, 15 % of

the population (83 million people) was located under drought affected areas during the 2003 event. . At the peaks of the largest droughts, the population located within areas under drought increases from 336 to 400 million people (Figure 4), and these numbers correspond to 61 % and 73 % of the European population, respectively. The increases in population within drought prone areas mostly occur in the Atlantic, Continental and Mediterranean region, because drought area is increasing the most in these regions (Table 1). Global warming may constitute human health threats<sup>31</sup> and extreme droughts, under particular situations, may trigger migration<sup>32</sup>. For these reasons, further studies should be conducted to investigate the potential effects of future extreme droughts on the European society and potential mitigation strategies aiming at reducing their negative effects.

Overall, Europe will face severe increases in the area affected by the largest soil moisture drought and the duration of such droughts if no adaptation is implemented during the coming decades. The magnitudes of these increases depend strongly on the level of global warming. . If future global temperatures will exceed 2 K above preindustrial levels<sup>11</sup>, our results show that drought areas will be up to 62 % larger under a warming level of 3 K compared to a warming level of 1 K. Similarly, the drought duration will increase by four times between these two warming levels. Decreases in aridity are found only in the Alpine and Boreal regions during the winter and spring. Even if adaptation measures are successfully implemented, aridity will increase throughout the continent during the summer from less than 10 mm at a global warming of 1.5 K to approximately

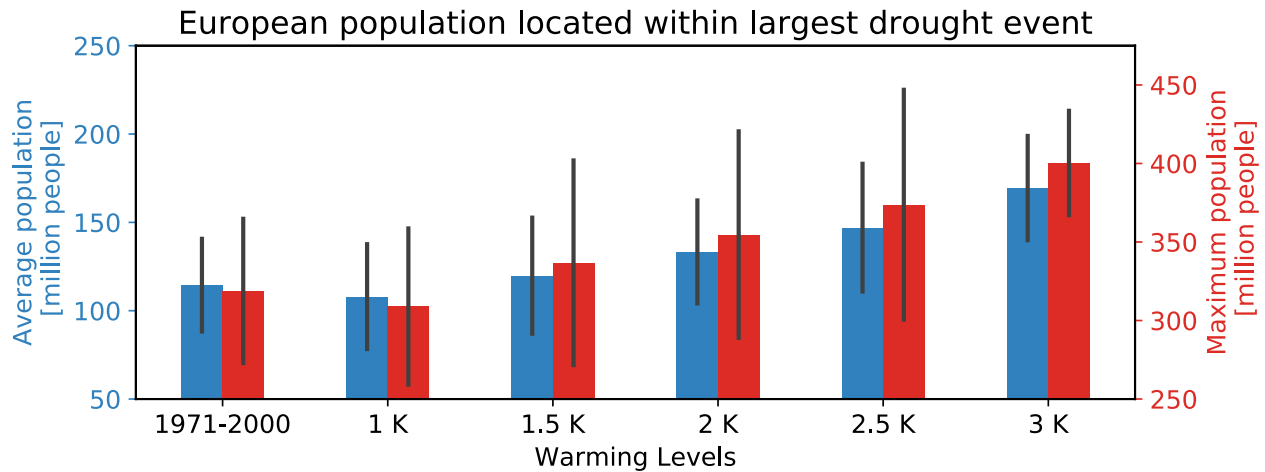


Figure 4: Average and maximum European population who are located within the area enduring the largest drought at a given warming level (i.e., experience an alteration in standard living conditions during an event). Population data for 2005 are used for reference, and these data were obtained from the SEDAC data set (<http://sedac.ciesin.columbia.edu>). Based on this data set, the population of the study area is estimated to be approximately 550 million people.

20-35 mm at a global warming of 3 K. Such an increase in aridity is comparable to the deficit during the 2003 drought event. Our study therefore highlights the need to adapt to new normal conditions to minimise the impact of extreme drought events. The European agricultural sector must adapt to summers with reduced soil water, and the risk of land degradation and desertification in sensitive environments exists. . Further research is urgently needed to assess the degree of impact of future extreme drought events on the European society as a whole, if increased aridity threatens minimum living conditions.<sup>32</sup>

## Methods

**Data and modelling chain** Daily temperature and precipitation values for the period 1950 to 2099 obtained from five Coupled Model Intercomparison Project v5 (CMIP5) Global Climate Models (GCMs) (HadGEM2-ES, IPSL-CM5A-LR, MIROC-ESM-CHEM, GFDL-ESM2M and NorESM1-M) forced by three RCPs (RCP2.6, RCP6.0, and RCP8.5) are used as input to four hydrologic models (HMs). These GCM data were made available by the ISI-MIP project<sup>24</sup> and are downscaled to a global resolution 0.5° and bias-corrected using a trend-preserving approach<sup>33</sup>. These models cover a range of 0.55 of the total uncertainty for precipitation and 0.75 for temperature<sup>34</sup>. The uncertainty range of this 5-member ensemble is comparable to that of a larger CMIP5 model ensemble (Figure S3)<sup>2</sup>. The 0.5° data are further disaggregated within the EDgE project ([edge.climate.copernicus.eu](http://edge.climate.copernicus.eu)) to a 5-km grid over Europe using the external drift kriging (EDK) approach. EDK estimates constitutes the best linear unbiased estimator of the selected meteorological variable. This key characteristic of EDK constraints the mean of the interpolated (downscaled) values to not differ from the expectation of the meteorological variable at this location. Thus, EDK does not introduce artefacts (e.g., trends) into the original forcing. Another advantage of this approach is that it introduces orographic effects of precipitation and temperature that are not present in GCMs at the coarse resolution, while maintaining the trend of the original data. The disadvantage of EDK is that it does not guarantee a conservation of mass and energy everywhere. Within the present study, however, the differences between original and downscaled values are in general



less than 1% (at most 5%) for precipitation and 0.1° C (at most 0.23° C) for temperature. These differences are smaller than the differences between the individual GCMs and the changes induced by climate change.

Two hydrological models (HMs) and two land surface models (LSMs) HMs (mHM, Noah-MP, VIC, and PCR-GLOBWB) are used to simulate soil moisture up to a depth of 2 m. The same morphologic, land cover, and soil data are used to setup these models; thus, the differences among the model simulations are due solely to differences in the representations of different processes used in the models. The mesoscale hydrological model (mHM; [www.ufz.de/mhm](http://www.ufz.de/mhm)) is a process-based hydrologic model that was developed for use at scales ranging from 1 km to 50 km<sup>35,36</sup>. PCR-GLOBWB was developed to represent the terrestrial water cycle, including artificial water management, at global and continental scales, and it places special emphasis on the groundwater component<sup>37</sup>. Noah-MP is the land-surface component of the Weather Research and Forecast model, and it represents both the terrestrial water and energy cycles<sup>38</sup>. VIC was developed to provide a simplified representation of land-surface hydrological processes that would be suitable for implementation in a GCM<sup>39</sup>. The model parameters are calibrated using the E-OBS meteorological data<sup>40</sup> for nine distinct catchments located in Spain, the United Kingdom, and Norway. An automatic calibration scheme is employed for mHM and PCR-GLOBWB<sup>41</sup>. Noah-MP is calibrated manually by adjusting the parameter describing surface evaporation resistance based on previous analyses<sup>42</sup>. The VIC parameters are taken from global simulation runs and are not calibrated using the E-OBS or observed river dis-

charge datasets over the EU domain.

**Model verification** Streamflow simulations from the four hydrologic models, driven by five GCMs, were compared against observations during the historical 30-year period (1966–1995). Here, we analyse the model skill for reproducing the median daily flows (p50) over 357 gauging stations located across the EU domain (Figure S4). Hydrologic model simulations are obtained using the forcings based on five GCMs during the period (1966-1995). The gauges have been selected from the Global Runoff Data Centre database. All gauges have complete 30-year period (1966–1995) of daily observations across the modelling domain, which allows for a robust statistical analysis. Additionally, these basins have an error of less than 10% in the basin delineation and the median basin area is 1680 km<sup>2</sup>. Overall, the ensemble model simulations show reasonably high skill in capturing the observed variability of p50, with a correlation coefficient value of 0.92 (Figure S4e) and the mean relative bias is 35%. In general, the model combinations (GCM/HM) appear to slightly overestimate the observed p50 values, with mHM being closest to observations compared to the Noah-MP, PCR-GLOBWB and VIC model simulations. The basins in the central EU region and in the Iberian peninsula generally exhibit a positive bias (Figure S4f). We note that these verifications are quite rigorous as the hydrologic models are forced with GCM simulated datasets, rather than observed meteorological datasets. This implies that a comparison of simulated and observed streamflow for specific time points is not feasible because GCM-based simulations do not reproduce observed weather and thus events.

**Estimation of warming levels** Within this study, the global warming levels for 1, 1.5, 2, 2.5, and 3 K are identified employing a time sampling approach<sup>15</sup>. The 30-year average temperature of 1971–2000 is used as a reference. The pre-industrial warming between the periods 1881–1910 and 1971–2000 is assumed to be 0.46 K<sup>43</sup>. This offset is subtracted from the warming levels for determining the 30-year periods for the specific global warming. These periods are identified as follows. For each general circulation model (GCM) and representative concentration pathway (RCP), calculate the 30-year global average temperature for all 30-year periods between 1960 and 2099 (prepending the historical data to each RCP). Note down the period when a 30-year global average temperature first reaches or exceeds a given global warming (1, 1.5, 2, 2.5, and 3 K minus 0.46 K offset)<sup>15</sup>. The procedure is illustrated in Figure S5 for all GCMs and RCPs. It is worth mentioning that other periods than 1881-1910 have been suggested to represent pre-industrial conditions, which might lead to offsets that are 0.11 K higher than the one used in this study<sup>44</sup>. We recalculated the periods based on this adjusted threshold and found shifts of 2 to 6 years (not shown). Given the fact that our analysis is using simulated soil moisture of 30 year periods, we expect little influence of the adjusted offset on our results.

In total, 15 GCM realisations reach 1 K, 14 reach 1.5 K, 13 reach 2 K, and 8 reach 2.5 K and 3 K global warming. As four HMs are used in this study, the obtained sample sizes are sufficiently large to quantify extreme soil moisture droughts for each level of global warming.

**Soil moisture index and drought characteristics** The soil moisture index SMI for a given cell and month is estimated as  $SMI_t = \hat{F}(x_t)$ , and it represents the quantile at the soil moisture fraction value  $x$  (normalised against the saturated soil water content).  $x_t$  denotes the simulated monthly soil moisture fraction at a time  $t$  and  $\hat{F}$  is the empirical distribution function estimated using the kernel density estimator  $\hat{f}(x)$  of the corresponding calendar month at time  $t$ .  $\hat{f}(x)$  is estimated as  $\hat{f}(x) = \frac{1}{nh} \sum_{k=1}^n K\left(\frac{x-x_k}{h}\right)$ . Here,  $x_1, \dots, x_n$  represents the simulated soil moisture fraction during a given calendar month during the reference period  $T$ ;  $n$  denotes the number of calendar months within a given period (i.e., 30 for a 30-year period); and  $K$  represents a Gaussian kernel function with a bandwidth  $h$ . The bandwidth is estimated by minimising a cross-validation error estimate<sup>20</sup> for the reference period separately for each calendar month, grid cell, LSM/HM and GCM combination to ensure comparability across time, space and model combinations. A cell at time  $t$  is under drought when  $SMI(t) < \tau$ . Here,  $\tau$  denotes that the soil water content in this cell is less than the values occurring  $\tau \times 100$  % of the time. In this study,  $\tau$  is set to 0.2. All drought events are identified using a multi-temporal clustering algorithm<sup>20</sup>. This algorithm first masks all cells at each time step that fulfil  $SMI \leq \tau$  and consolidates adjacent cells to a drought event. Second, drought events at consecutive time steps that share a minimum overlapping area are consolidated into a single event. Third, drought statistics (e.g., areal extent, duration, and magnitude) are estimated for all identified drought events. The *mean duration* ( $D$ ) of a drought event is then defined as the mean of the drought duration estimated over every cell affected by a drought event. This statistic is

given in months. The *mean areal extent* ( $A$ ) is defined as the average of the region under drought from the onset until the end of the drought event, which is then expressed as a percentage of the total surface area of the region. It should be noted that the value of the threshold  $\tau$  certainly determines  $A$  and  $D$ . Sensitivity analysis, however, shows that the rate of increase of these characteristics between two warming levels is invariant of the value of  $\tau$  (compare Figure 1 and Figure S1). The soil moisture drought threshold  $\hat{F}_T^{-1}(\tau)$  is estimated in two ways to quantify the effect of adaptation to climate change: 1)  $T$  is chosen as 1971-2000 to calculate the drought area and duration for all warming levels, which represents no adaptation to climate change, 2)  $T$  is identical to the period when a global warming level has been reached, which represents adaptation to climate change<sup>14</sup>. In the latter case, it depends on the amount of global warming, the GCM and the RCP considered.

**Estimation of available soil water (aridity)** The changes in the water soil storage (aridity) that occur at the different warming levels is estimated by varying the reference period from  $T_0$  to  $T_\Delta$ , where  $T_0$  denotes the historical reference period (1971–2000), and  $T_\Delta$  denotes the period until a particular value of  $\Delta K$  is reached in a given RCP and GCM combination. Based on these two periods, the change in aridity within a region (as represented by the average over all of the cells within the region) for a given RCP-GCM-HM combination is estimated as  $\delta x_\Delta = \overline{\langle \hat{F}_{T_\Delta}^{-1}(\tau) \rangle} - \overline{\langle \hat{F}_{T_0}^{-1}(\tau) \rangle}$ . The operator  $\langle \cdot \rangle$  denotes the ensemble mean, and the overline indicates the spatial average. Finally, the seasonal averages are estimated from the values obtained for each month. This index is depicted in

Figure 3. Note that the threshold  $\tau$  is kept constant (e.g., 0.2) for  $T_0$  and  $T_\Delta$ . The absolute soil moisture thresholds (e.g,  $\hat{F}_{T_\Delta}^{-1}(\tau)$ ), on the other hand, depend on the period.

**Estimation of soil water deficit for the 2003 event** For a given drought event occurring in a period  $T$ , the soil water deficit in a given grid cell is estimated by  $d_i^T(t) = \left[ \hat{F}_{T,i}^{-1}(\tau) - x_i(t) \right]_+$ . The average deficit estimated over the lifespan of a drought event occurring in a period  $T$  is given as  $d^T = \frac{1}{n_T} \overline{\sum_{t \in T} d_i^T(t)}$ . Here,  $n_T$  denotes the number of months under drought in the period  $T$  and the overline indicates the spatial average. The operator  $[\cdot]_+$  denotes the positive part function. The soil water deficit for the 2003 event is estimated as indicated above with every hydrological model forced with the E-OBS<sup>40</sup> meteorological data (1950–2015). The period  $T$  corresponds to 1960–2002. The ensemble average is afterwards estimated and reported.

**Comparison of SMI and PDSI** Numerous studies on drought research used the Palmer Drought Severity Index (PDSI)<sup>1,6,23,45</sup>. The PDSI is a water budget accounting index that cumulates soil moisture anomalies derived from monthly precipitation and temperature. Here, we use the self-calibrating version of PDSI<sup>46</sup> at the monthly timescale. PDSI requires two input parameters for every grid cell. These are the latitude of the considered location and the available water holding capacity (AWC). The latter is derived using the same soil dataset used for the hydrologic models and the Multiscale Parameter Regionalization (MPR) method used in the mesoscale Hydrologic Model (mHM)<sup>35</sup>. The calibration period for the PDSI is set to 1971 to 2000, which is consistent with the period for the estimation of the kernel density function of the soil moisture index (SMI) Subsequently,

both indices (SMI and PDSI) are evaluated during the period 2010 to 2099. We present results for one location in Eastern Germany (lat: 51.09 °N, lon: 12.89 °E) to discuss the differences between the PDSI and the SMI. However, the same features discussed below were also observed at locations in Southern France, Spain, and England.

The RCP 2.6 scenario results in stationary SMI and PDSI data without any significant trend (Figure S6). This can be expected because the RCP 2.6 scenario leads to a projected increase in global mean temperature of 0.3-1.7 K until the end of the 21st century. All indices detect relatively more droughts under RCP 6.0 (Figure S7) and RCP 8.5 (Figure S8) as compared to RCP 2.6. However, there are substantial differences between the PDSI and SMI. Most importantly, the median PDSI is indicating extreme drought conditions for the last third of the 21st century for both RCP 6.0 and RCP 8.5. In the latter case, the median PDSI shows a strong negative trend. For the same period, the median SMI is indicating non-drought conditions for the majority of time points. This indicates that the PDSI is extremely sensitive to the projected climate change in this region. It is worth noting that climate change in this region is mostly increasing temperature, whereas annual precipitation is increased by less than 10% (Figure S2). It is known that the PDSI method using the temperature-based Thornthwaite potential evapotranspiration scheme is oversensitive to changes in temperature and that the Penman-Monteith method provides a less biased estimate<sup>23</sup>. The hydrologic models mHM and PCR-GLOBWB also use a temperature-based PET formulation (i.e., the Hargreaves-Samani equation<sup>47</sup>), but show a similar behaviour as Noah-MP and VIC (Figures S6, S7, S8), which do not use a

PET approach and calculate the full energy balance at the land surface.

23

These results highlight that the combination of a temperature-based PET approach with the conceptualisation of the PDSI leads to an overestimation of drought conditions. On the contrary, a drought index derived from hydrologic models (i.e., mHM and PCR-GLOBWB) that use a temperature-based PET scheme, do not exhibit such behaviour. The reason for such difference stems from the way these indices are estimated. PDSI is an autoregressive model of the type  $X_t = pX_{t-1} + qZ_t$  that estimates the current PDSI value ( $X_t$ ) based on the previous value of the index and the current soil moisture anomaly  $Z_t$ <sup>46</sup>. Here  $p$  and  $q$  are the so-called Palmer “duration” factors to be determined empirically for every location.  $Z_t$  is determined with a two layer water balance model and several empirically parameters that “allow for accurate comparisons of PDSI values over time and space”<sup>46</sup>. The autoregressive conceptualisation of PDSI under a non-stationary climate (i.e., increasing temperature, PET, and soil moisture anomalies under RCP6.0, RCP8.5) induces a negative drift from the long-term mean. On the contrast, SMI is by definition bounded between zero and one because it corresponds to the respective quantiles of the simulated soil moisture (see Section above).

23

**Drought frequencies related to changes of meteorological forcings** Figure S9 provides a comparison of the number of drought months for the individual hydrologic models,



considering no adaptation to climate change for various levels of global warming. All hydrologic models show a similar increase in drought frequency in the Mediterranean region in southern Europe. This may be related to the relatively large decrease in annual precipitation of up to 25% at a warming level of 3 K (Figure S2). In central Europe, all models exhibit a smaller increase of drought frequencies in comparison to those in the Mediterranean, which can be expected given the relatively smaller changes in projected precipitation (Figure S2). Projected temperature is increasing similarly in central Europe and the Mediterranean region, which highlights that the simulated evapotranspiration in this model ensemble is limited by water availability rather than by energy in this region. In contrast, precipitation is projected to increase in the Scandinavian region in northern Europe up to 20%. In this region, the hydrologic models differ in their projections of drought frequencies. For example, VIC and mHM show increases in this region, PCR-GLOBWB shows a mixed pattern, and drought frequencies simulated by Noah-MP remain unchanged by global warming. Because all models are forced with the same meteorological data, the parameterization of snow processes in this cold region and the parameterization of ET have a strong impact on soil drought characteristics. For example, mHM allows ET when the surface is covered with snow, which is based on the model assumption that snow cover has a large subgrid variability. On the contrary, Noah-MP assumes that the snow cover is evenly distributed over the entire grid cell preventing any evaporation. These results show that the hydrological models have relative larger differences over various regions. For this reason, we consider it fundamental to use a multi-model ensemble for

climate change drought analysis.

**Population in drought areas** For each member of the multi-model ensemble, the spatio-temporal evolution of the largest drought event is identified during the reference period  $T_0$  and all of the 30-year periods representing different levels of global warming  $T_\Delta$ . This information is then overlaid with the population density to estimate the population located in the area under drought at a given point in time. Based on these results, we estimate the average and maximum populations affected over the lifespan of the drought. To identify the effect of future droughts, we use the distribution of the population of Europe in 2005. The UN-adjusted Gridded Population of the World, data set, version 4, was obtained from SEDAC (<http://sedac.ciesin.columbia.edu>). The year 2005 is selected because it best represents the population distribution during the 2003 event, which is used in this study as a reference. According to this data set, the population of the entire domain is approximately 550 million people. This analysis does not account for demographic changes.

1. Dai, A., Trenberth, K. & Qian, T. A global dataset of Palmer Drought Severity Index for 1870-2002: Relationship with soil moisture and effects of surface warming. *Journal of Hydrometeorology* **5**, 1117–1130 (2004).
2. Greve, P., Gudmundsson, L. & Seneviratne, S. I. Regional scaling of annual mean precipitation and water availability with global temperature change. *Earth System Dynamics Discussions* 1–24 (2017).

3. Hirschi, M. *et al.* Observational evidence for soil-moisture impact on hot extremes in southeastern Europe. *Nature Geoscience* **4**, 17–21 (2010).
4. Dai, A. Increasing drought under global warming in observations and models. *Nature Climate Change* **3**, 52–58 (2013).
5. Seneviratne, S. I. *et al.* Impact of soil moisture-climate feedbacks on CMIP5 projections: First results from the GLACE-CMIP5 experiment. *Geophysical Research Letters* **40**, 5212–5217 (2013).
6. Trenberth, K. E. *et al.* Global warming and changes in drought. *Nature Climate Change* **4**, 17–22 (2014).
7. Huang, J., Yu, H., Guan, X., Wang, G. & Guo, R. Accelerated dryland expansion under climate change. *Nature Climate Change* **3**, 847–854 (2015).
8. Berg, A., Sheffield, J. & Milly, P. C. D. Divergent surface and total soil moisture projections under global warming. *Geophysical Research Letters* **44**, 236–244 (2017).  
URL <http://dx.doi.org/10.1002/2016GL071921>. 2016GL071921.
9. Cook, B. I., Ault, T. R. & Smerdon, J. E. Unprecedented 21st century drought risk in the American Southwest and Central Plains. *Science Advances* **1**, e1400082–e1400082 (2015).
10. UNFCCC. Adoption of the Paris agreement, Proposal by the President. Tech. Rep., United Nations, Geneva, Switzerland (2015).

11. Raftery, A. E., Zimmer, A., Frierson, D. M. W., Startz, R. & Liu, P. Less than 2C warming by 2100 unlikely. *Nature Climate Change* **109**, 13915–7 (2017).
12. Collins, M. *et al.* Quantifying future climate change. *Nature Climate Change* **2**, 403–409 (2012).
13. Prudhomme, C. *et al.* Hydrological droughts in the 21st century, hotspots and uncertainties from a global multimodel ensemble experiment. *Proceedings of the National Academy of Sciences* **111**, 3262–3267 (2014).
14. Wanders, N., Wada, Y. & Van Lanen, H. A. J. Global hydrological droughts in the 21st century under a changing hydrological regime. *Earth System Dynamics* **6**, 1–15 (2015).
15. James, R., Washington, R., Schleussner, C.-F., Rogelj, J. & Conway, D. Characterizing half-a-degree difference: a review of methods for identifying regional climate responses to global warming targets. *Wiley Interdisciplinary Reviews-Climate Change* **8**, 1–23 (2017).
16. Wilhite, D. Drought as a natural hazard: concepts and definitions. In Wilhite, D. (ed.) *Drought: A Global Assessment, Vol. I*, chap. 1, 3–18 (Routledge, London, 2000).
17. Moore, F. C. & Lobell, D. B. Adaptation potential of European agriculture in response to climate change. *Nature Climate Change* **4**, 610–614 (2014).
18. Van Lanen, H. A. *et al.* Hydrology needed to manage droughts: the 2015 European case. *Hydrological Processes* **30**, 3097–3104 (2016).

19. Ciais, P. *et al.* Europe-wide reduction in primary productivity caused by the heat and drought in 2003. *Nature* **437**, 529–533 (2005).
20. Samaniego, L., Kumar, R. & Zink, M. Implications of Parameter Uncertainty on Soil Moisture Drought Analysis in Germany. *Journal of Hydrometeorology* **14**, 47–68 (2013).
21. Samaniego, L. *et al.* Propagation of forcing and model uncertainties on to hydrological drought characteristics in a multi-model century-long experiment in large river basins. *Climatic Change* **141**, 435–449 (2016).
22. Lehner, F. *et al.* Projected drought risk in 1.5°C and 2°C warmer climates. *Geophysical Research Letters* **44**, 7419–7428 (2017).
23. Sheffield, J., Wood, E. F. & Roderick, M. L. Little change in global drought over the past 60 years. *Nature* **491**, 435–438 (2012).
24. Warszawski, L. *et al.* The Inter-Sectoral Impact Model Intercomparison Project (ISI-MIP): Project framework. *Proceedings of the National Academy of Sciences* **111**, 3228–3232 (2014).
25. Samaniego, L. EDgE model chain and development of Sectoral Climate Impact Indicators. Online <http://edge.climate.copernicus.eu> (2017). Last visited, 11.09.2017.
26. Kovats, R. *et al.* Europe. In Barros, V. *et al.* (eds.) *Climate Change 2014: Impacts, Adaptation, and Vulnerability. Part B: Regional Aspects. Contribution of Work-*

- ing Group II to the Fifth Assessment Report of the Intergovernmental Panel on Climate Change*, 1267–1326 (Cambridge University Press, Cambridge, United Kingdom and New York, NY, USA, 2011).
27. Metzger, M. J., Bunce, R. G. H., Jongman, R. H. G., Múcher, C. A. & Watkins, J. W. A climatic stratification of the environment of Europe. *Global Ecology and Biogeography* **14**, 549–563 (2005). URL <http://dx.doi.org/10.1111/j.1466-822X.2005.00190.x>.
  28. Rötter, R. P., Carter, T. R., Olesen, J. E. & Porter, J. R. Crop–climate models need an overhaul. *Nature Climate Change* **1**, 175–177 (2011).
  29. Guiot, J. & Cramer, W. Climate change: The 2015 Paris Agreement thresholds and Mediterranean basin ecosystems. *Science* **354**, 465–468 (2016).
  30. Seneviratne, S. I., Donat, M. G., Pitman, A. J., Knutti, R. & Wilby, R. L. Allowable CO<sub>2</sub> emissions based on regional and impact-related climate targets. *Nature* **529**, 477–483 (2016).
  31. Robine, J.-M. *et al.* Death toll exceeded 70,000 in Europe during the summer of 2003. *Comptes Rendus Biologies* **331**, 171 – 178 (2008). Dossier : Nouveautés en cancérogenèse / New developments in carcinogenesis.
  32. Wilbanks, T. *et al.* Industry, settlement and society. In Parry, M., Canziani, O., Palutikof, J., van der Linden, P. & Hanson, C. (eds.) *Climate Change 2007: Impacts, Adaptation and Vulnerability. Contribution of Working Group II to the Fourth Assessment*

- Report of the Intergovernmental Panel on Climate Change*, 357–390 (Cambridge University Press, Cambridge, UK, 2007).
33. Hempel, S., Frieler, K., Warszawski, L., Schewe, J. & Piontek, F. A trend-preserving bias correction - the ISI-MIP approach. *Earth System Dynamics* **4**, 219–236 (2013).
  34. McSweeney, C. F. & Jones, R. G. How representative is the spread of climate projections from the 5 CMIP5 GCMs used in ISI-MIP? *Climate Services* **1**, 24–29 (2016).
  35. Samaniego, L., Kumar, R. & Attinger, S. Multiscale parameter regionalization of a grid-based hydrologic model at the mesoscale. *Water Resources Research* **46**, W05523 (2010).
  36. Kumar, R., Samaniego, L. & Attinger, S. Implications of distributed hydrologic model parameterization on water fluxes at multiple scales and locations. *Water Resources Research* **49**, 360–379 (2013).
  37. van Beek, L. P. H., Wada, Y. & Bierkens, M. F. P. Global monthly water stress: 1. Water balance and water availability. *Water Resources Research* **47**, n/a–n/a (2011).
  38. Niu, G.-Y. *et al.* The community Noah land surface model with multiparameterization options (Noah-MP): 1. Model description and evaluation with local-scale measurements. *Journal of Geophysical Research* **116** (2011).
  39. Liang, X., Lettenmaier, D., Wood, E. & Burges, S. A Simple Hydrologically Based Model of Land-Surface Water and Energy Fluxes for General-Circulation Models. *Journal of Geophysical Research-Atmospheres* **99**, 14415–14428 (1994).

40. Haylock, M. R. *et al.* A European daily high-resolution gridded data set of surface temperature and precipitation for 1950–2006. *Journal of Geophysical Research: Atmospheres (1984–2012)* **113** (2008).
41. Rakovec, O. *et al.* Multiscale and Multivariate Evaluation of Water Fluxes and States over European River Basins. *Journal of Hydrometeorology* **17**, 287–307 (2016).
42. Cuntz, M. *et al.* The impact of standard and hard-coded parameters on the hydrologic fluxes in the Noah-MP land surface model. *Journal of Geophysical Research: Atmospheres* **121**, 10,676–10,700 (2016).
43. Vautard, R. *et al.* The European climate under a 2 degrees C global warming. *Environmental Research Letters* **9** (2014).
44. Hawkins, E. *et al.* Estimating Changes in Global Temperature since the Preindustrial Period. *Bulletin of the American Meteorological Society* **98**, 1841–1856 (2017).
45. Palmer, W. C. Meteorological drought (1965).
46. Wells, N., Goddard, S. & Hayes, M. J. A self-calibrating Palmer Drought Severity Index. *Journal of Climate* **17**, 2335–2351 (2004).
47. Hargreaves, G. H. & Samani, Z. A. Reference Crop Evapotranspiration from Temperature. *Applied engineering in agriculture* **1**, 96–99 (1985).

**Acknowledgements** This study was partially performed under a contract for the Copernicus Climate Change Service ([edge.climate.copernicus.eu](http://edge.climate.copernicus.eu)). ECMWF implements this service and the



Copernicus Atmosphere Monitoring Service on behalf of the European Commission. This study has been mainly funded within the scope of the HOKLIM project ([www.ufz.de/hoklim](http://www.ufz.de/hoklim)) by the German Ministry for Education and Research (grant number 01LS1611A). We would like to thank people from various organisations and projects for kindly providing us the data which were used in this study, which includes ISI-MIP, JRC, NASA, GRDC, BGR & ISRIC. This study was carried out within the Helmholtz-Association climate initiative REKLIM ([www.reklim.de](http://www.reklim.de)).

**Author contributions** L.S. and S.T. designed the study and wrote the manuscript; S.T., R.K., N.W., and M.P. conducted the model runs. O.R. and M.Z. conducted analysis of data. All authors contributed to interpreting results.

**Additional information** Supplementary information is available in the online version of the paper. Reprints and permissions information is available online at [www.nature.com/reprints](http://www.nature.com/reprints). Correspondence and requests for materials should be addressed to L.S.

**Competing Financial Interests** The authors declare that they have no competing financial interests.

**Table 1:** Multi-model ensemble median results for the area under drought ([% of total area]), drought duration [months], and months under drought conditions per year for different levels of global warming and stratified for the IPCC regions. The period of 1971–2000 is used as a reference.

Warming level	Atlantic	Continental	Boreal	Mediterr.	Alpine North	Alpine South
Drought area						
Reference	21.9	34.7	19.4	28.2	41.3	28.9
1.0 K	24.0	36.8	25.2	29.8	31.8	28.7
1.5 K	23.5	35.1	24.7	34.1	34.5	28.7
2.0 K	22.8	35.8	23.4	38.4	34.8	29.4
2.5 K	26.5	36.1	23.0	41.0	35.9	34.4
3.0 K	27.8	39.9	16.4	49.1	41.1	37.1
Drought duration						
Reference	31.5	32.5	25.0	28.0	12.0	37.0
1.0 K	32.0	38.5	25.0	41.0	22.0	40.0
1.5 K	52.5	60.0	25.0	58.0	20.5	56.0
2.0 K	60.5	65.5	32.5	71.0	21.0	68.5
2.5 K	84.0	86.5	41.5	89.0	18.5	86.5
3.0 K	101.5	121.5	59.5	125.0	17.0	124.5
Drought months per year						
Reference	2.0	2.0	1.9	2.1	1.9	2.0
1.0 K	2.0	2.1	2.0	2.6	1.7	1.9
1.5 K	2.7	2.6	2.4	3.2	1.9	2.3
2.0 K	3.0	2.8	2.5	3.7	2.0	2.7
2.5 K	3.3	3.1	2.7	4.5	2.2	3.2
3.0 K	3.8	3.9	2.9	5.6	2.4	3.9

**Supplementary Material for**

**Climate change induces extreme soil droughts in Europe**

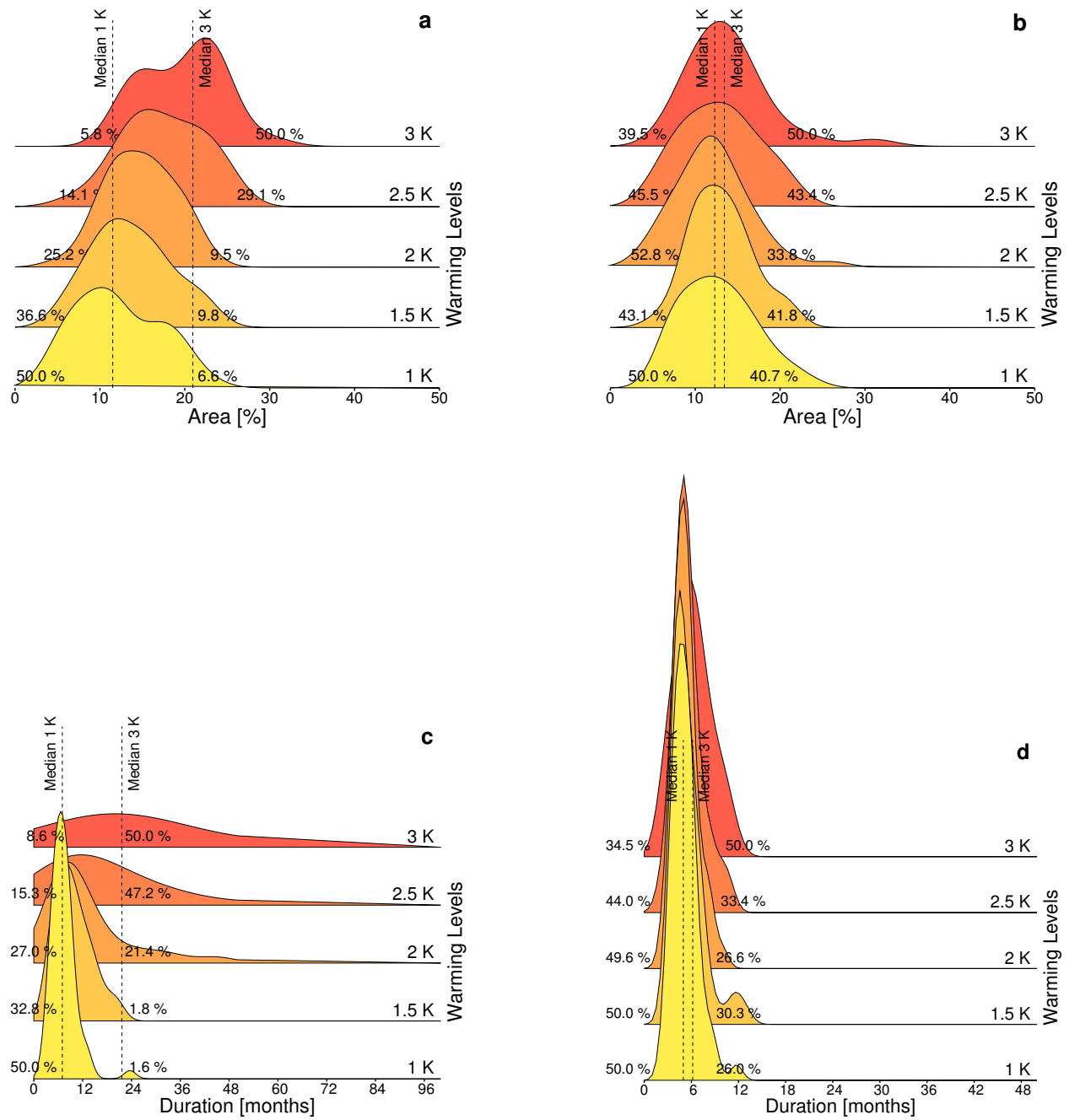


Figure S1: Same as Figure 1 in the main text, but using a drought threshold of 0.1 for the spatio-temporal clustering algorithm.

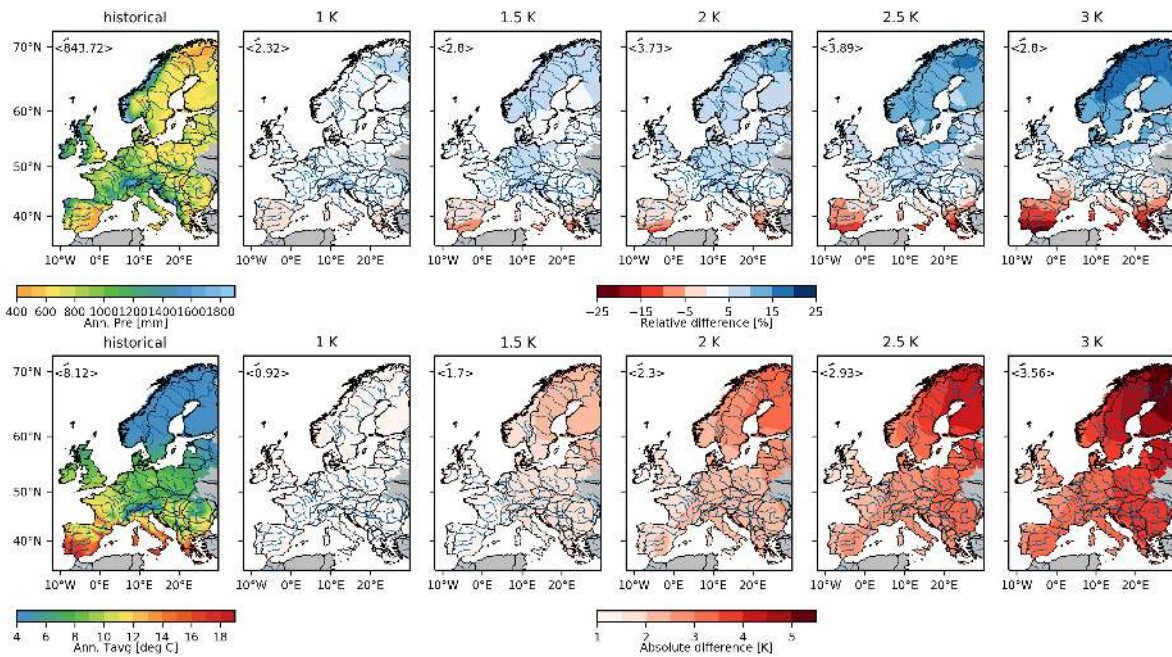


Figure S2: Upper panels show the historical annual average precipitation for the reference period and the corresponding anomalies for various global warming levels. Lower panels show the same but for annual average temperature.

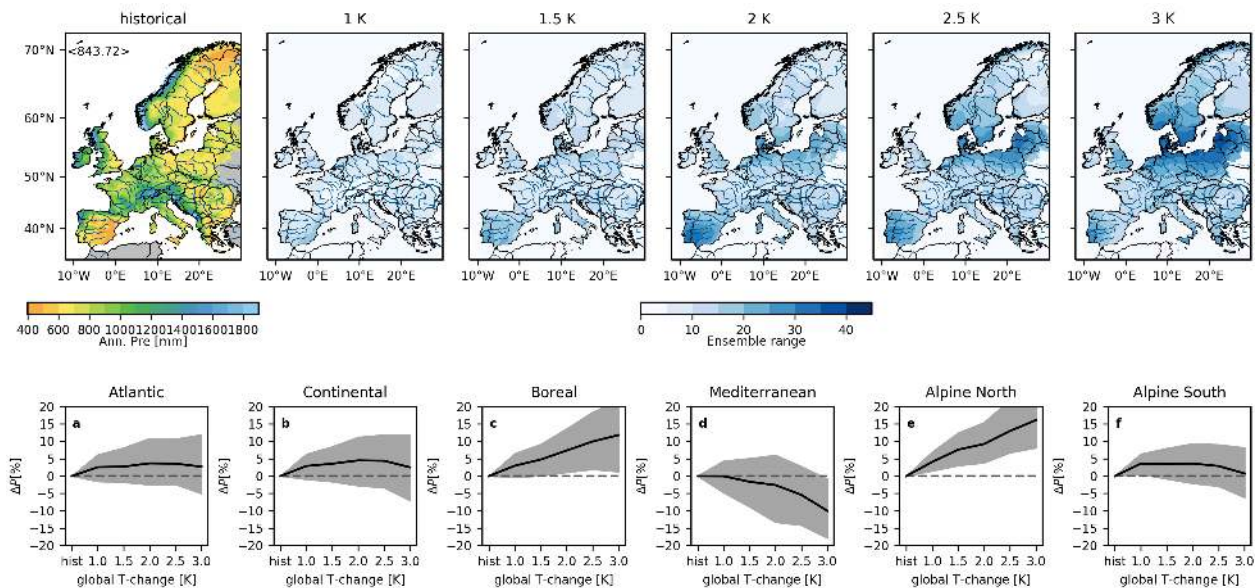


Figure S3: In the top row, the map for the historical period shows the long-term annual precipitation of the 5 GCMs used in this study. For the different warming levels, the map show the ensemble range between the percentage change occurring with a probability of 90% and 10% according to the five GCMs used under three RCPs. These values are then averaged for the different European regions and depicted in the lower row.

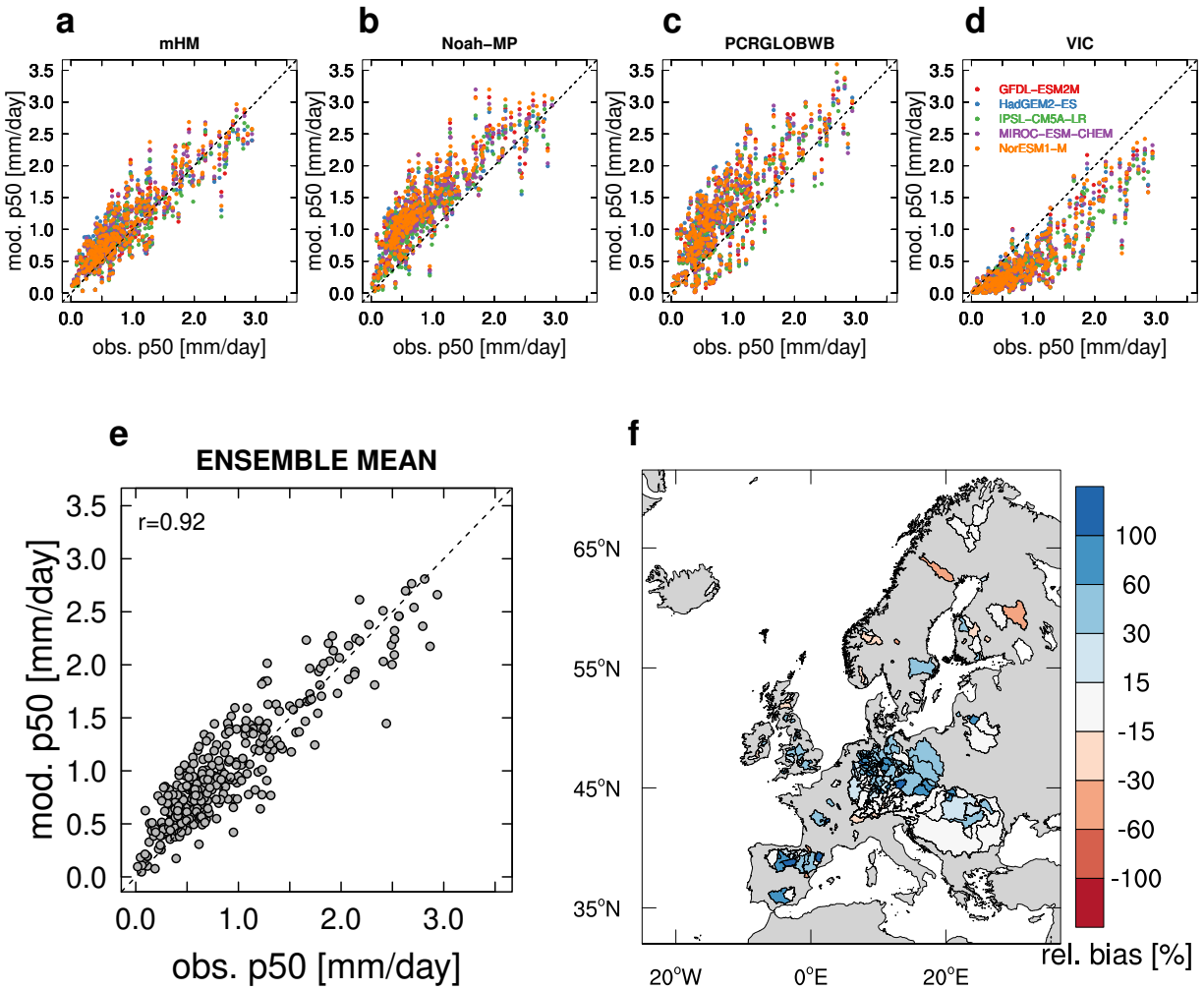


Figure S4: Scatter plots of the median daily streamflow (p50) between observations and simulations for individual GCM/HM combinations (panels a to d) and the multi-model mean (panel e). Hydrologic model simulations are obtained using the forcings based on five GCMs during the period (1966-1995) over 357 EU river basins. Also shown are geographical location of the river basins with colours indicating relative bias between simulations and observations (panel f).

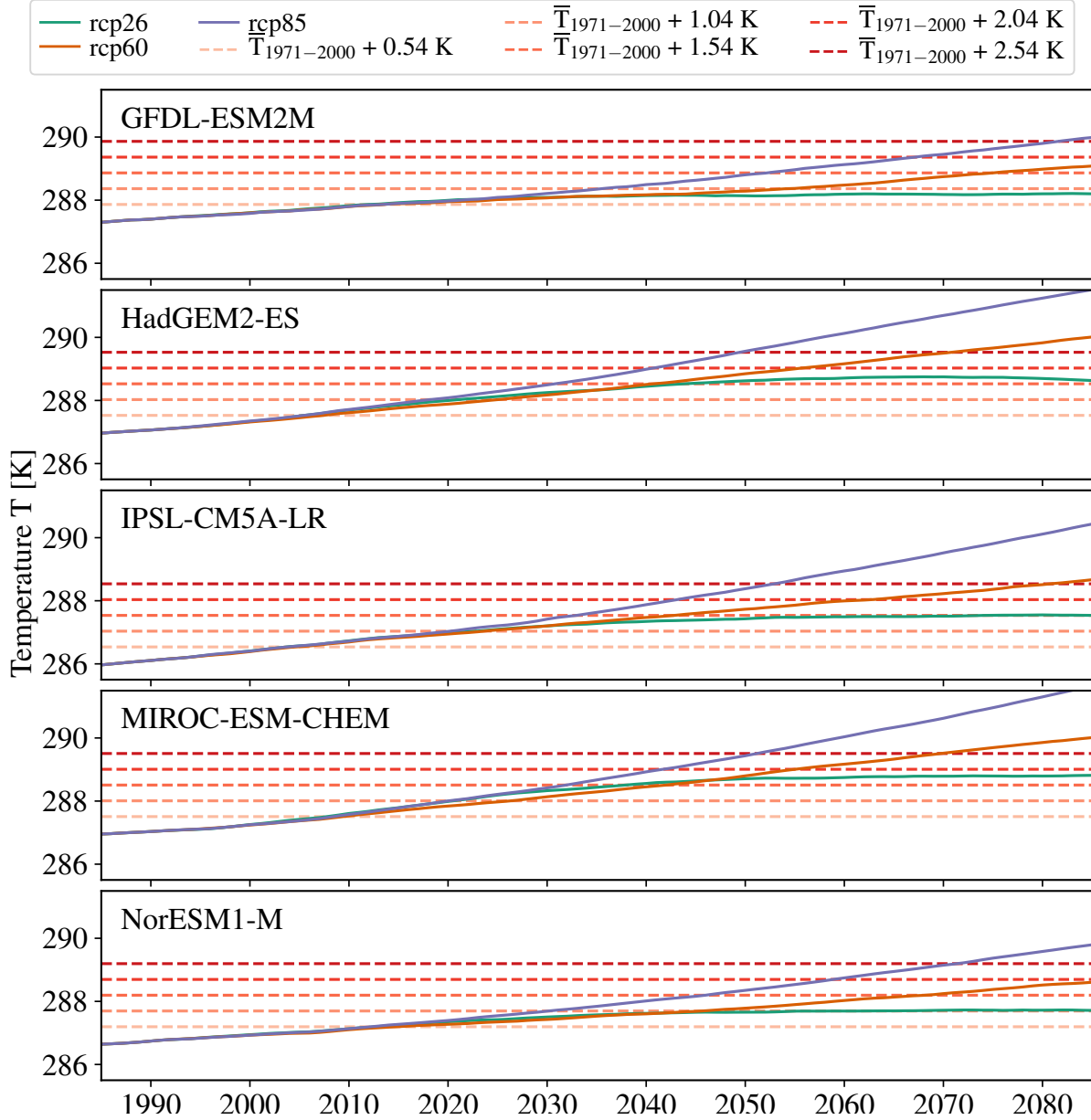


Figure S5: Development of centered 30-year global average temperatures for all five General Circulation Models (GCMs) included in this study. The horizontal lines mark when the global warming of 1, 1.5, 2, 2.5, and 3 K are reached. The coloured lines indicate the different Representative Concentration Pathways (RCPs): RCP2.6, RCP6.0, and RCP8.5.



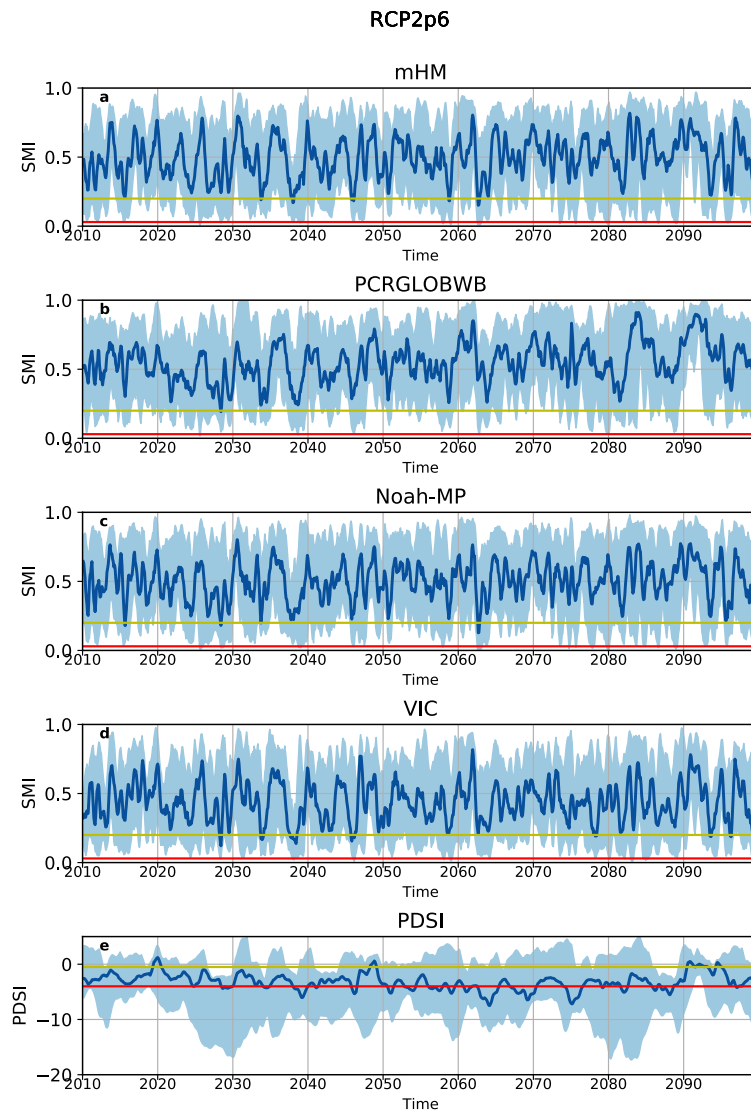


Figure S6: Panels a) to d): Soil moisture index (SMI) of the four hydrologic models used in this study for one location in Eastern Germany (Saxony). Each panel contains five realizations under RCP 2.6 (one for each considered General Circulation Model, GCM). For clarity, only the median (solid blue line) and the range from minimum to maximum are shown. Panel e): Same as a) to d), but for PDSI instead of a hydrologic model. For both indices SMI and PDSI, red and yellow lines depict thresholds for drought events having an exceedance probability of 95% and 80%, respectively.

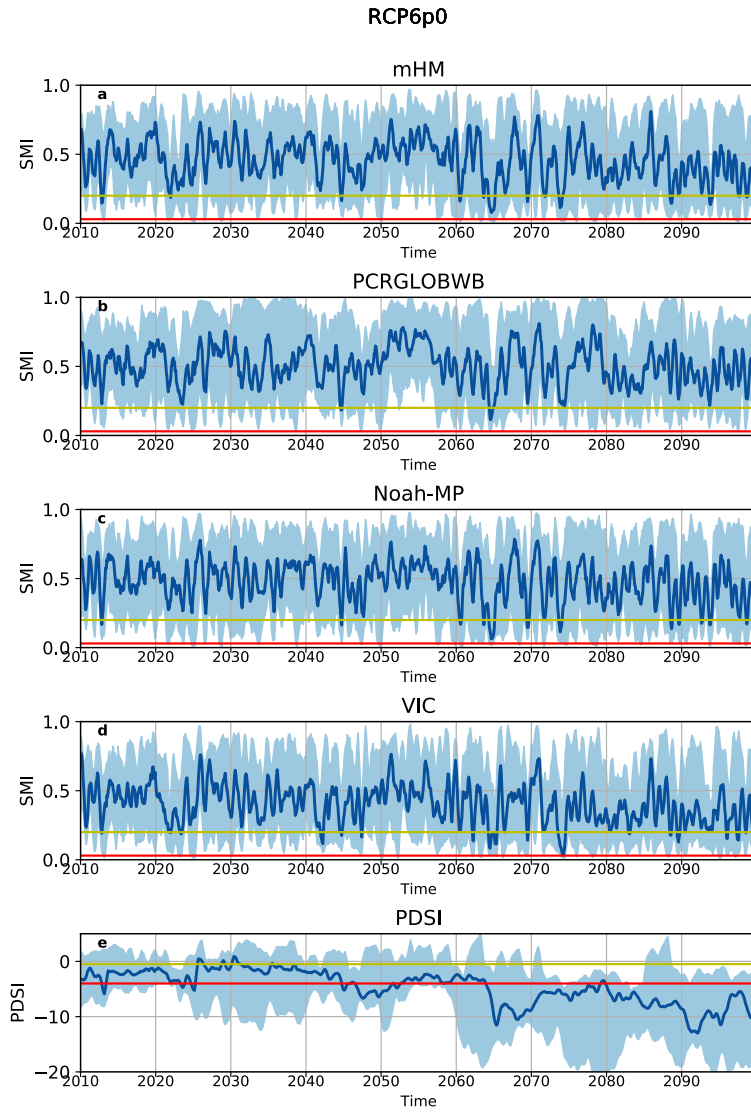


Figure S7: Same as Figure S6, but for RCP 6.0.

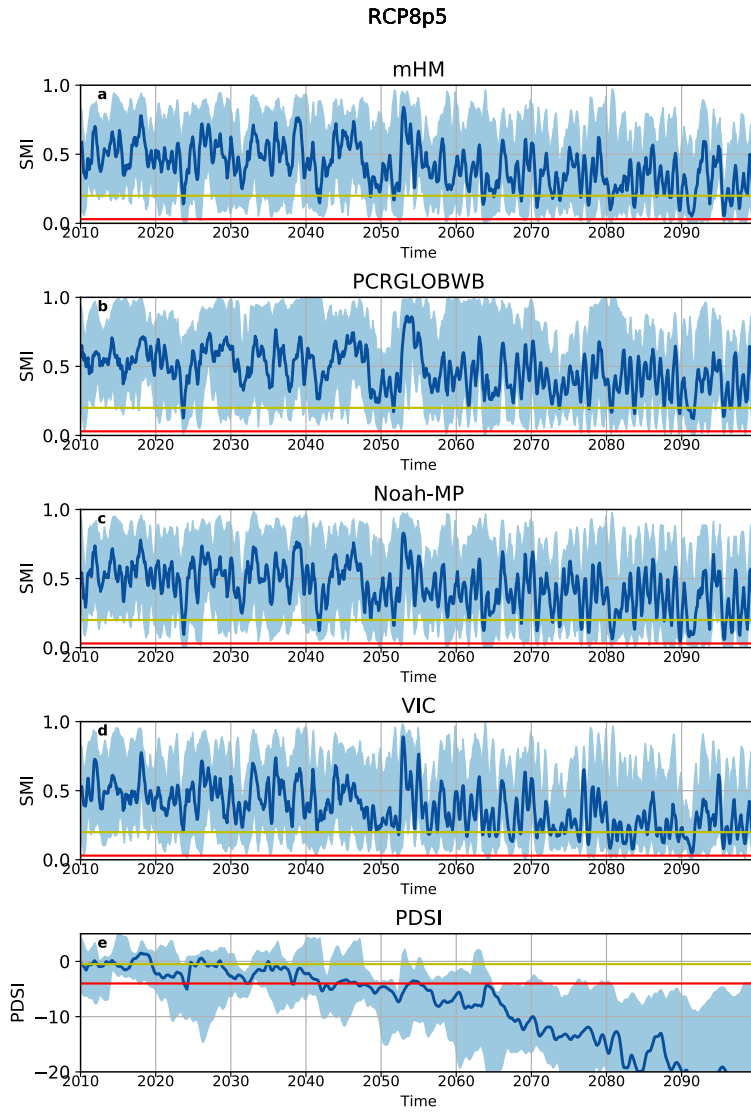


Figure S8: Same as Figure S6, but for RCP 8.5.

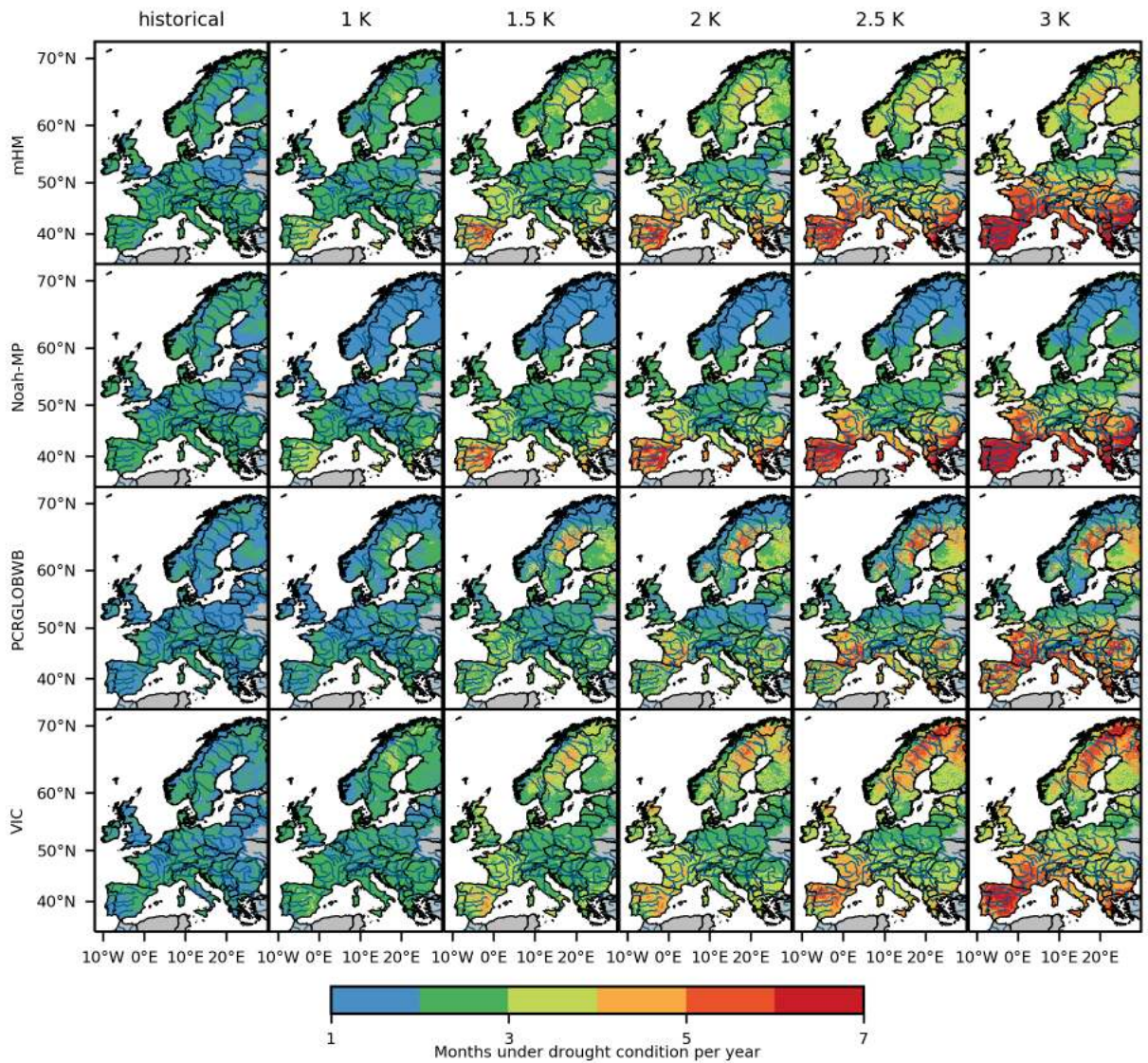


Figure S9: Estimation of the drought frequency (months per year) estimated for every hydrological model for various global warming levels. The number of drought months per year are calculated using the distribution functions of the SMI of the reference period, thus assuming no adaptation to climate change.